Reproducibility of Liquid Micro-Flow Measurements

J. D. Wright and J. W. Schmidt

National Institute of Standards and Technology (NIST), 100 Bureau Drive, Gaithersburg, MD, USA 20899
E-mail: john.wright@nist.gov

New applications in biology, medicine, and manufacturing require reliable measurements of liquid flows smaller than 100 µL/min. NIST addressed this requirement by improving the reliability and ease of use of NIST's Dynamic Gravimetric Micro-Flow Standard. The meter under test is now connected to the weighing beaker by a liquid bridge that reduces variations in parasitic surface tension forces as the level of liquid in the collection beaker rises. We describe other improvements to NIST's standard (e.g. pipette positioning and evaporation reduction) and provide an uncertainty analysis for the present system. The gravimetric standard measures liquid flow between 0.1 µL/min and 100 µL/min with uncertainty ranging from 4.5 % to 0.04 %. Repeated calibrations of five commercially available micro-flow meters (one for nearly 2 years) show that their calibrations are reproducible within 1.5 % for many months.

1. Introduction

The NIST Fluid Metrology Group (FMG) builds and operates liquid flow standards that are used to calibrate flow meters and to conduct flow research. In 2014, the FMG began building a flow standard for flows of 1 mL/min and smaller [1]. The micro-flow standard uses the dynamic gravimetric flow method, *i.e.*, it periodically records the time and the mass of liquid accumulating in a beaker resting on a weigh scale (balance) and calculates the rate of change of mass with respect to time (the mass flow). This document explains the method of flow measurement in detail, gives an uncertainty analysis, and presents calibration data for five flow meters.

2. NIST Dynamic Gravimetric Micro-Flow Standard: Equipment and Operation

The arrangement of equipment used in NIST's Dynamic Gravimetric Micro-Flow Standard (DGMFS) is shown in Figures 1 and 2. A computer-controlled Cetoni* Nemesys syringe pump is used as the source (or sink) of water. The system is filled with water by withdrawing the syringe while a three-way valve connects the syringe to a reservoir of pure, filtered water. Once the syringe is fully withdrawn, the three-way valve is turned so that the syringe pump pushes the water into the downstream tubing of the DGMFS, thereby pushing air out of the system. The water flows though a Systec 2.5 mL active de-bubbler. Air bubbles in the flow that reach the de-bubbler pass though a Poridex gas permeable membrane to a vacuum pump. The test section can hold several meters under test (MUTs) while recording their flow indications. Translucent plastic tubing (1.6 mm or 0.8 mm inside diameter) conducts the water between components and enables detecting air bubbles in the system. The tubing is terminated by a 0.5 mm heat-drawn glass pipette that delivers water to or from a beaker that rests on a Sartorious balance (6 g full scale, 0.1 µg. resolution).

---

* Certain commercial entities, equipment, or materials may be identified in this document in order to describe an experimental procedure or concept adequately. Such identification is not intended to imply recommendation or endorsement by the National Institute of Standards and Technology, nor is it intended to imply that the entities, materials, or equipment are necessarily the best available for the purpose.
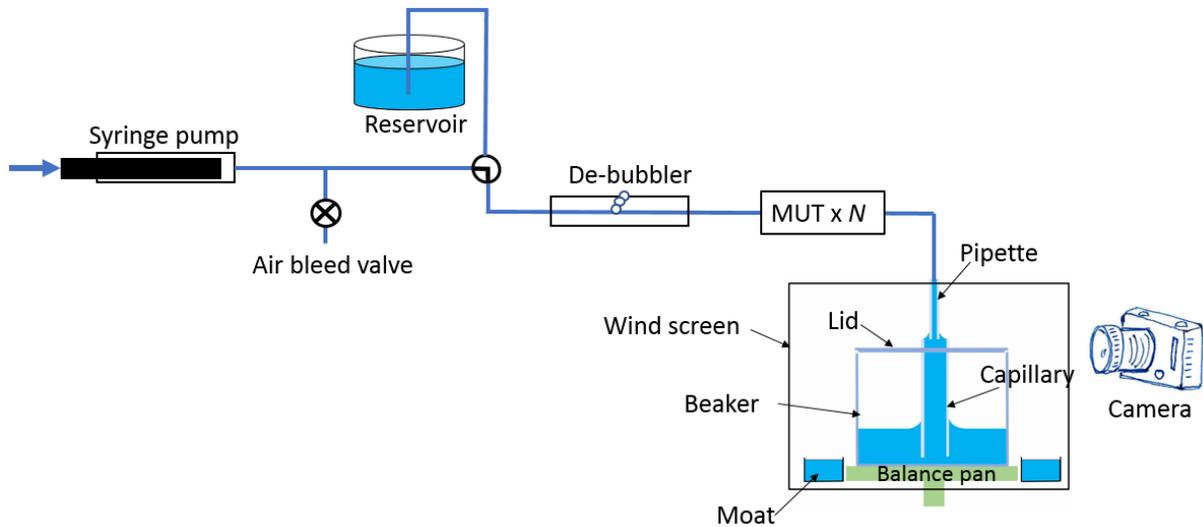
Figure 1. Sketch of the Dynamic Gravimetric Micro-Flow Standard (DGMFS).
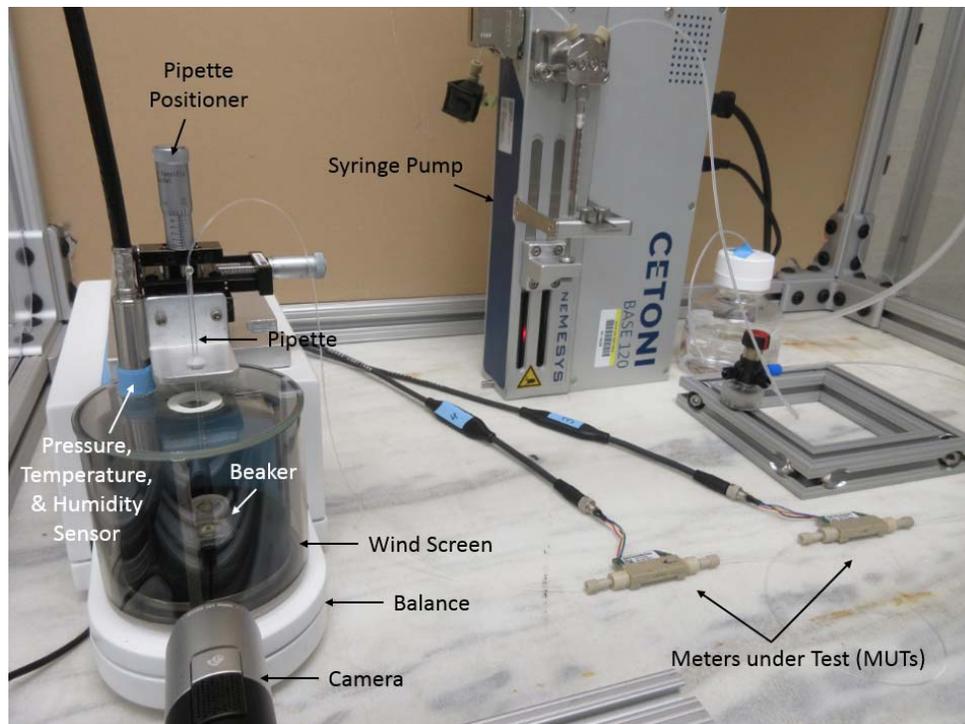

Figure 2. Overview of the DGMFS showing the syringe pump, connecting tubing, meters under test, and the 6 g balance.

Figures 3 and 4 show the equipment on or near the balance pan. The weighed beaker has a lid with a 1.5 mm diameter capillary passing though its center. The capillary is attached to the lid and does not reach the bottom of the beaker, so the water can flow into or out of the capillary. The beaker's lid is not air-tight;

therefore, air moves in and out of the beaker as the water level changes, but the lid does reduce evaporation of the collected water. Using a 3-axis linear stage, the pipette is positioned so that its tip is inside the capillary but it does not touch the capillary's walls. A camera provides a magnified view of the pipette / capillary interface to facilitate pipette positioning. Capillary action pulls water to the top of the capillary and once the pipette is filled and properly positioned, a liquid bridge forms between the pipette and the capillary. The water surface at the interface between the pipette and the capillary remains nearly stationary as water fills or is removed from the beaker.
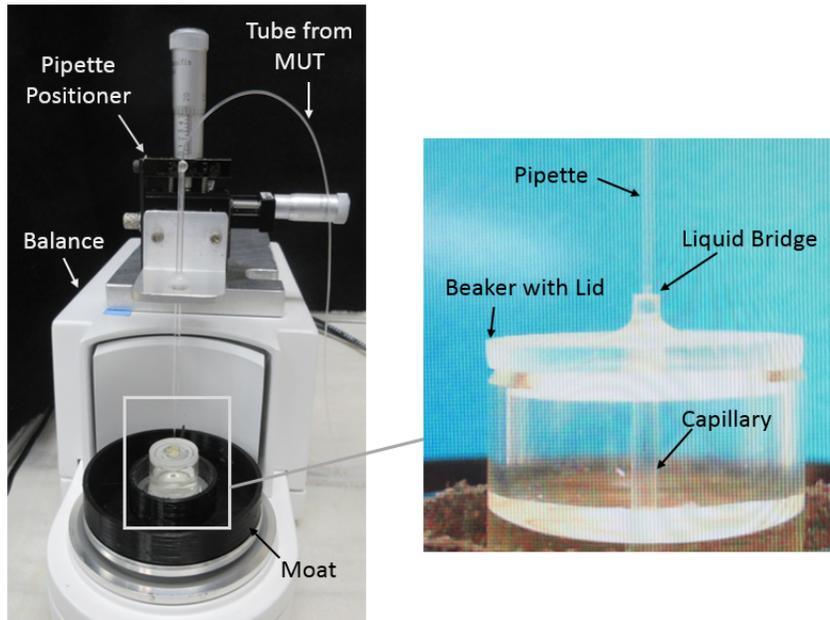

Figure 3. Left: Photograph of the balance (without wind screen installed), beaker, and pipette positioning system. Right: A close-up view of the beaker and the fluid coupling between the pipette and capillary.
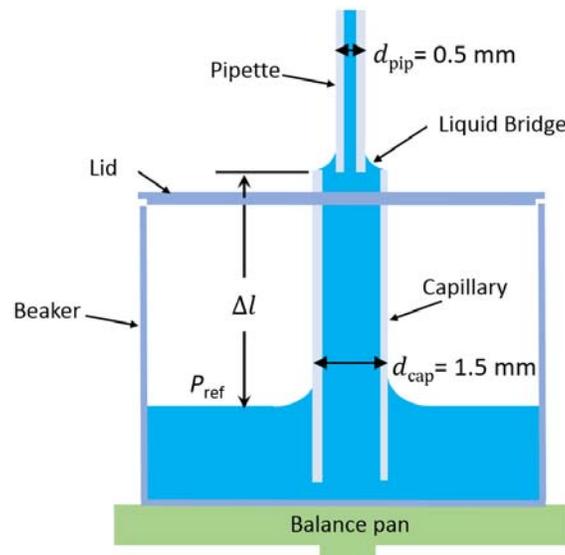

Figure 4. The beaker, capillary, and pipette used to weigh liquid in the dynamic gravimetric micro-flow standard.

The balance pan has a wind screen to block air currents that might alter the balance readings (installed in Figure 2, removed in Figure 3). A small open reservoir of water (a moat) under the wind screen (but not on the balance pan) comprises an "evaporation trap": water vapor from it maintains approximately 90 % relative humidity under the wind screen and reduces evaporation from the liquid bridge and beaker. The pipette passes though a small hole in the wind screen. The pressure, temperature, and relative humidity of the air under the wind screen is measured in order to make buoyancy corrections for the mass of water in the beaker. The environmental conditions in the lab are stable to ± 1 °C. The DGMFS is enclosed in a plexiglass enclosure, further dampening air currents and temperature fluctuations.

A data acquisition computer and Labview program control the DGFMS, acquire mass, time, and other necessary sensor readings, and process the data to calculate flow. Flow set points are established via the syringe pump, or optionally via the elevation of a water reservoir attached to a vertical stage. The empty collection beaker weighs 4 g, so the beaker can be filled with up to 2 g of water before reaching the 6 g capacity of the balance. During normal operation, the beaker is filled with approximately 2 mL of water so that it weighs just under 6 g initially and the water supply is moved back and forth between the beaker and the syringe pump, producing negative and positive flows at the meter under test. We wait 5 minutes or more for flow stability after each set point change and then take five one-minute-long averages from the DGMFS and the MUT. Longer stabilization times and averages are used at lower flows. Upon completion of the flow set points, data are recorded at the zero flow condition (stopped syringe pump) to gravimetrically measure the evaporation from the beaker. A sample data set is shown in Figure 5.
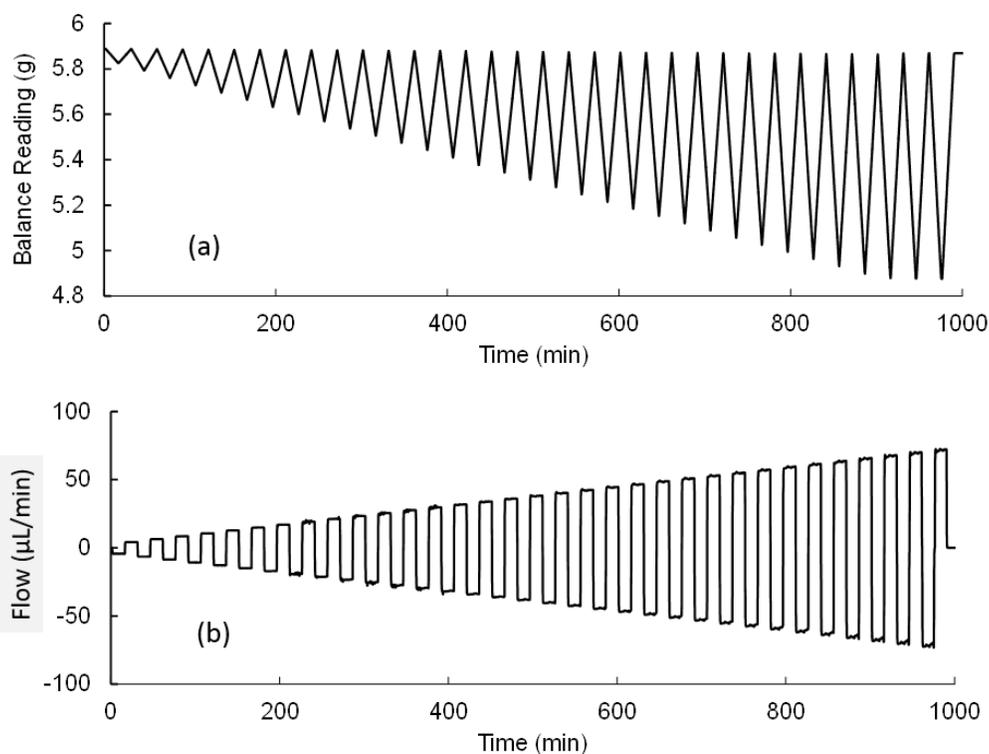

Figure 5. Mass versus time (a) and flow ($\mathrm{d}m/\mathrm{d}t$) versus time (b) for a calibration made with the DGMFS.

3. DGMFS Flow Equations

The DGMFS measures the mass flow though the meter under test from the time rate of change of the mass of water in the collection beaker. A force balance shows that corrections for buoyancy forces and

evaporation are necessary to obtain low uncertainty flow measurements. The forces imposed between the beaker and the balance pan are depicted in Figure 6. In Figure 6, each force has been divided by the gravitational acceleration g so that the quantities have units of mass.

- The quantity F_{bal}/g is the opposing force provided by the balance pan to the beaker and its contents divided by g. The balance software applies a correction for buoyancy using assumed values for the density of the weighed object and the surrounding air. To remove this buoyancy correction and obtain F_{bal}/g, it is necessary to multiply the balance reading by $1 - \rho_{\text{air}*}/\rho_{\text{std}} = 0.99985$, where $\rho_{\text{air}*}$ is the density of air assumed by the balance software (0.0012 g/cm³) and ρ_{std} is the assumed density for a stainless steel mass standard (8 g/cm³).

- Surface tension at the liquid interface between the pipette and the capillary produces an upward force equal to the product of the circumference of the pipette $\pi\, d_{\text{pip}}$, the surface tension γ, and the cosine of the liquid contact angle θ_{liq} (hereafter assumed equal to zero).

- The buoyancy forces of the water collected in the beaker and the beaker itself lead to the terms $V_{\text{liq}}\,\rho_{\text{air}}$ and $V_{\text{beaker}}\,\rho_{\text{air}}$ where V_{liq} and V_{beaker} are the volumes of the water and beaker respectively, and ρ_{air} is the density of the surrounding air. Note that ρ_{air} is not assumed to be a constant; it is calculated using [2] and the pressure, temperature, and relative humidity measured near the balance pan.

- The pressure at the tip of the pipette is lower than the atmospheric pressure (P_{ref}) by the hydrostatic head of the water between the top of the capillary and the main body of water in the beaker (Δl in Figure 4). The beaker and its contents are partially supported by this small pressure difference ($\rho\, \Delta l\, g \approx 150$ Pa). The supporting force ($\rho_{\text{liq}}\, \Delta l\, A_{\text{pip}}$) is a function of the depth of the water in the beaker.

- m and m_{beaker} are the masses of the water in the beaker and of the beaker itself. Note that for the purposes of the force balance, the beaker lid and the capillary are part of the beaker.

- The term $V_{\text{pip}}\,\rho_{\text{liq}}$ accounts for buoyancy forces imposed on the balance due to the tip of the pipette in the water within the capillary.
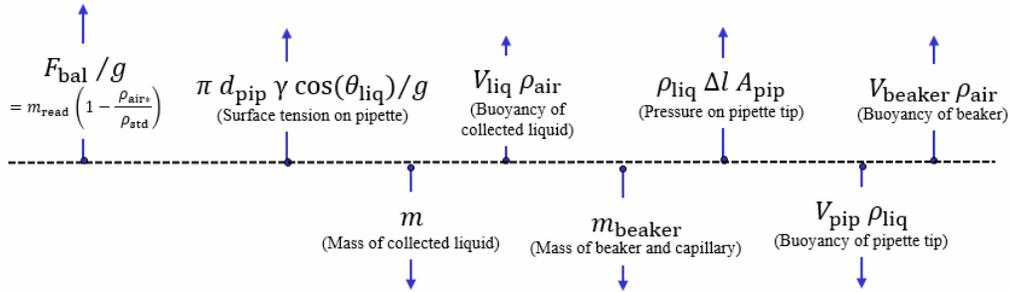

Figure 6. Contributions to the force balance on the beaker. The magnitudes of the vectors are not drawn to scale.

Setting the sum of the terms in Figure 6 equal to zero and solving for the mass of water in the beaker at a particular time gives:

$$m = \frac{F_{\text{bal}}}{g} + \frac{\pi\, d_{pip}\, \gamma}{g} + V_{\text{liq}}\,\rho_{\text{air}} + \rho_{\text{liq}}\, \Delta l\, A_{\text{pip}} + V_{\text{beaker}}\,\rho_{\text{air}} - m_{\text{beaker}} - V_{\text{pip}}\,\rho_{\text{liq}}. \tag{1}$$

Using the relationships $F_{\text{bal}}/g = m_{\text{read}}\left(1 - \frac{\rho_{\text{air}*}}{\rho_{\text{std}}}\right)$ and $V_{\text{liq}} = m/\rho_{\text{liq}}$ leads to:

$$m = m_{\text{read}}\frac{\left(1 - \frac{\rho_{\text{air}*}}{\rho_{\text{std}}}\right)}{\left(1 - \frac{\rho_{\text{air}}}{\rho_{\text{liq}}}\right)} + \rho_{\text{liq}}\, \Delta l\, A_{\text{pip}} + \frac{\pi\, d_{pip}\, \gamma}{g} + V_{\text{beaker}}\,\rho_{\text{air}} - m_{\text{beaker}} - V_{\text{pip}}\,\rho_{\text{liq}}. \tag{2}$$

The mass flow can be calculated from the difference in mass of the beaker contents divided by the time between the two mass measurements. Several of the forces represented in Equation 2 are effectively constant over time and will cancel when a mass change is calculated, i.e., $\pi d_{pip} \gamma / g$, $V_{\text{beaker}} \rho_{\text{air}}$, m_{beaker}, and $V_{\text{pip}} \rho_{\text{liq}}$. (Note that the cancelling terms *will* be considered as sources of uncertainty.) Assuming that the density of the water and of the surrounding air remains constant, the mass change Δm between two mass measurements m_1 and m_2 is:

$$\Delta m = \Delta m_{\text{read}} \frac{\left(1 - \frac{\rho_{\text{air}*}}{\rho_{\text{std}}}\right)}{\left(1 - \frac{\rho_{\text{air}}}{\rho_{\text{liq}}}\right)} + \rho_{\text{liq}} A_{\text{pip}} \left(\Delta l_2 - \Delta l_1\right) . \tag{3}$$

The change in the level of water in the beaker can be closely approximated using the change in reading of the balance and the cross-sectional areas of the beaker and capillary:

$$\Delta l_2 - \Delta l_1 \cong -\frac{\Delta m_{\text{read}}}{\rho_{\text{liq}}(A_{\text{beaker}} - A_{\text{cap}})} \frac{\left(1 - \frac{\rho_{\text{air}*}}{\rho_{\text{std}}}\right)}{\left(1 - \frac{\rho_{\text{air}}}{\rho_{\text{liq}}}\right)}, \text{ which leads to:} \tag{4}$$

$$\Delta m \cong \Delta m_{\text{read}} \frac{\left(1 - \frac{\rho_{\text{air}*}}{\rho_{\text{std}}}\right)}{\left(1 - \frac{\rho_{\text{air}}}{\rho_{\text{liq}}}\right)} \left[1 - \frac{A_{\text{pip}}}{(A_{\text{beaker}} - A_{\text{cap}})}\right] . \tag{5}$$

In review, the expression $\left(1 - \frac{\rho_{\text{air}*}}{\rho_{\text{std}}}\right)$ removes buoyancy corrections for stainless steel reference masses implemented by the balance software and the term $\left(1 - \frac{\rho_{\text{air}}}{\rho_{\text{liq}}}\right)$ corrects for buoyancy forces on the collected water. The term in the square brackets (the pipette hydrostatic correction) accounts for hydrostatic or pressure forces on the pipette tip that change as the water level changes in the beaker.

To calculate the mass flow from two mass measurements, one could divide the change in mass by the time interval between m_1 and m_2. But we can reduce the effects of random variations in the mass measurements and balance uncertainties by calculating the rate of change of mass from a larger number of mass and time values. Equation 6 gives the slope of the mass-versus-time record as determined using a first order least squares regression [3] with N pseudo-mass values $\hat{m}$ evenly spaced in time, t

$$\dot{m}_0 = \frac{d\hat{m}}{dt} \cong \frac{N \sum_{j=1}^{N} t_j \hat{m}_j - \sum_{j=1}^{N} t_j \sum_{j=1}^{N} \hat{m}_j}{N \sum_{j=1}^{N} t_j^2 - \left(\sum_{j=1}^{N} t_j\right)^2} . \tag{6}$$

A pseudo-mass value $\hat{m}$ can be used to calculate the 0th order mass flow:

$$\hat{m} = m_{\text{read}} \frac{\left(1 - \frac{\rho_{\text{air}*}}{\rho_{\text{std}}}\right)}{\left(1 - \frac{\rho_{\text{air}}}{\rho_{\text{liq}}}\right)} . \tag{7}$$

The 0th order mass flow is then corrected by 1) the hydrostatic or pressure effect on the pipette tip and 2) evaporation:

$$\dot{m} = \dot{m}_0 \left[1 - \frac{A_{\text{pip}}}{(A_{\text{beaker}} - A_{\text{cap}})}\right] + \frac{dm_{\text{evap}}}{dt} . \tag{8}$$

The evaporation correction is based on measurements made under zero flow conditions and will be discussed in more detail later in this paper.

The volumetric flow at the meter under test (MUT) can be calculated from the mass flow and the density at the MUT via:

$$Q = \frac{\dot{m}}{\rho_{\text{liq}}} \quad .$$

(9)

The density of the water depends on the temperature and the pressure of the water, so formally, the water density in the beaker and at the MUT (ρ_{liq} in equations 7 and 9 respectively) are not equal. However for the temperature uniformity and pressures in our laboratory, the water density differences are negligible compared to other uncertainty sources.

Note that Equation 1 applies to a beaker with an interface as shown in Figure 4, i. e., a system utilizing a liquid bridge so that the liquid does not rise on the externally supported pipette as the beaker fills. In an earlier version of the NIST micro-flow standard, the filling tube was directly inserted into the liquid collecting in the beaker, and an additional correction was necessary to account for increasing buoyancy forces exerted by the tube on the balance as the liquid rises around the tube [1]. A micro-flow standard that has the liquid level rising around the pipette is subject to changes in the surface tension forces imposed on the balance due to "stick-slip" behaviour of the liquid / pipette interface [1]: the liquid meniscus often varies in shape as the liquid level changes due to the pipette's surface inhomogeneities.

4. DGFMS Uncertainty Analysis

The approximately 95 % confidence level ($k = 2$) uncertainty of the DGMFS for flows between 0.1 µL/min and 100 µL/min is plotted in Figure 7. At the largest flows, the uncertainty is dominated by the repeatability of the best MUT known to us and by the pipette hydrostatic correction. Below 1 µL/min, uncertainty in the corrections made for evaporation and the repeatability of the best-available MUT dominate. Table 1 lists the uncertainty components, nominal values for the quantities, their uncertainty, and the contribution of each component to the total uncertainty for a 100 µL/min flow. In the following sections, the broad uncertainty categories listed in Table 1 and their estimations are discussed.

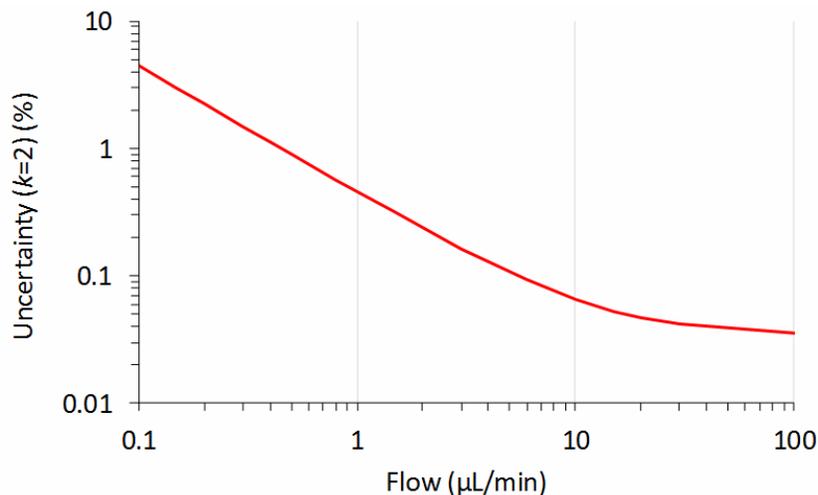**Figure 7.** The 95 % confidence level uncertainty of the DGMFS versus flow.

Table 1. Uncertainty of the DGMFS for a flow of 100 µL/min.

Uncertainty category	Value	Units	Standard unc. ($k = 1$)	Contrib.
			(%)	(%)
ΔMass with buoyancy corr.	0.1	[g]	0.003	0
ΔTime	1	[min]	0.002	0
Pipette hydrostatic corr.	0.999	[-]	0.008	19
Slope calculation	0	[g/min]	0	0
Evaporation	-0.01	[µL/min]	0.002	1
Water density	0.998	[g/cm³]	0.005	0
Repeatability & flow stability	0.1	[g/min]	0.016	79
Expanded uncertainty ($k = 2$)	0.04	[µL/min]	0.04	

Change in Mass (with Buoyancy Corrections): At low flows, the largest contributor to the mass change uncertainty is zero drift of the balance. At high flows, the largest contributor is gain (slope) errors in the balance calibration. Uncertainty due to the resolution of the balance (0.1 µg) is small compared to the zero drift and gain errors. Buoyancy corrections are significant (0.12 %), but their uncertainty (< 5 parts in 10^6) is not significant, thanks to the low uncertainty of the sensors and equations used for air density.

Balance zero drift is indistinguishable from changes in the mass of the beaker due to water flowing into it. Zero drift data were collected by placing a reference mass on the balance pan (with the wind screen in place) and using the data acquisition system to record the balance readings. Figure 8 shows an example data set. The line shows the balance readings over a 15 hour interval and the symbols are one minute averages of the flow (or drift) calculated as done for flow calibrations. For the data in Figure 8, the largest drift value is 0.26 µg/min and the standard deviation of the drift is 0.08 µg/min. The maximum slopes observed in this (and other) data sets were used to quantify the standard uncertainty (68 % confidence level) due to zero drift (0.16 µg/min).
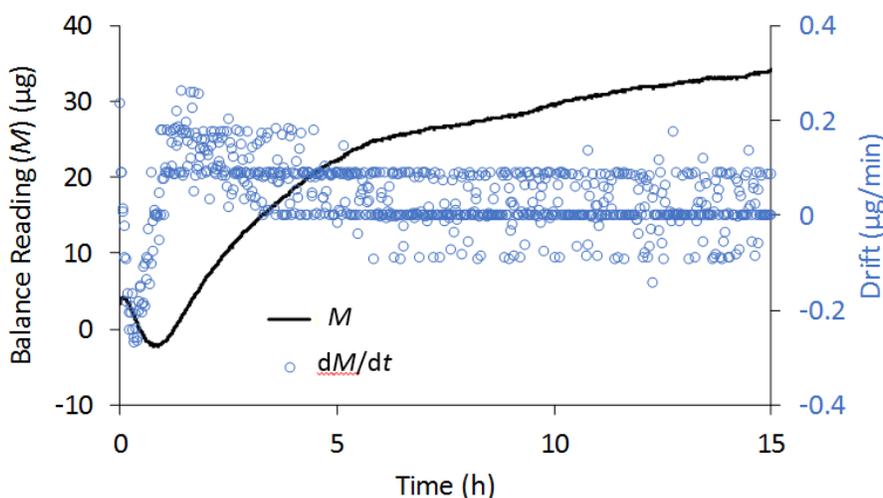

Figure 8. The balance reading during a 15 h interval and one minute averages of its slope (drift). This and additional, similar data sets were used to quantify the standard uncertainty of the drift in the balance calibration: 0.16 µg/min (0.16 nL/min).

The balance is periodically calibrated using the procedure provided by the manufacturer, i.e. the zero and gain of the balance are adjusted by automatically placing an internal reference mass on or off the balance. We verified this internal calibration process by placing reference masses between zero and 6 g (in 1 g increments) on the balance and comparing the balance readings to the known reference mass values. On occasion, the reference-mass verifications were conducted 4 months after an internal calibration to reveal how well the balance holds its calibration over time. Based on the data in Figure 9, we conclude that the balance gain error and calibration stability can introduce 0.03 mg uncertainty ($k = 1$) for each gram of mass change measured.
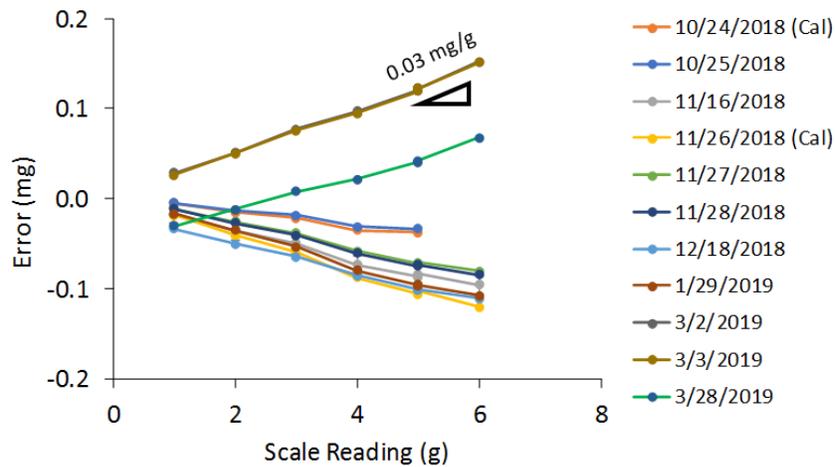
Figure 9. Results of balance calibrations performed using reference masses. Internal scale calibrations were performed on the dates followed by the notation (Cal) in the legend.

Change in Time: Mass values are acquired from the balance at 2.5 Hz. The uncertainty of the time values attributed to the mass measurements has two main sources: 1) drift in the clock of the computer that is used for data acquisition, and 2) inconsistencies in the time for communication between the balance and the computer (latency). The computer clock drift is periodically checked by disconnecting it from the computer network to prevent automatic time corrections and visually comparing the computer clock to a cell phone clock over a 72 h interval. These periodic checks show that the computer clock is correct with standard uncertainty of 20 parts in 10^6.

We assessed the time uncertainties introduced by variations in the digital communications between the balance and the computer (latency) from the standard deviation of the period of the data acquisitions. The period measured via Labview timing functions (i.e. the data acquisition computer clock) is 0.39861 s and it has a standard deviation of 75 µs. For the minimum flow data collection time (60 s), this is a standard uncertainty of 1 part in 10^6. Combining clock drift and latency components gives a standard uncertainty for the time measurements of 20 parts in 10^6.
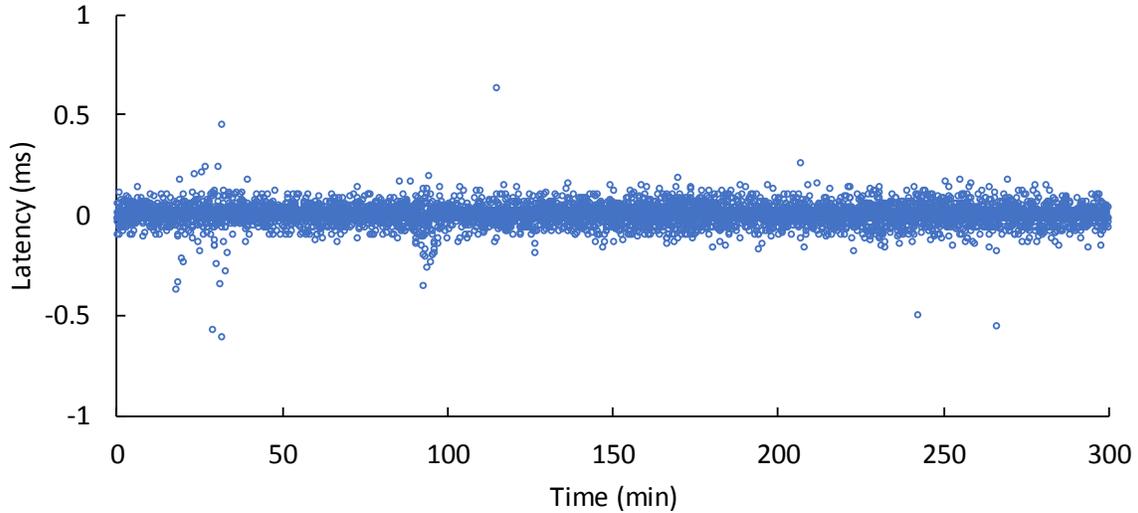
Figure 10. Variations in the communication time (latency) for the data acquisition computer and the balance. The standard deviation of data like these were used in the time uncertainty analysis.

Pipette Hydrostatic Correction: This correction accounts for the force on the balance caused by the pressure difference at the top of the capillary relative to the atmospheric pressure. The correction depends on the dimensions of the beaker, capillary, and pipette. Of these dimensions, the correction is most sensitive to uncertainty of the pipette's inside diameter, known with a standard uncertainty of 0.02 mm which leads to a standard uncertainty of 80 parts in 10^6 in the correction.

Slope Calculation: The slope of the mass-time data pairs is calculated via Equation 6 using a 20 s long moving window of data collected at 2.5 Hz. The mass flow values from the slope calculation (and the acquired output of the MUT) are averaged for a minimum of 60 s, so the effective minimum number of data points fitted is $N = 150$. At flows < 1 µL/min, the averaging time is lengthened to produce mass changes greater than 1 mg to control uncertainty due to balance resolution (0.1 µg). The uncertainty in the mass values (and associated corrections) is at least 2.5 times larger than the uncertainty in the time values, allowing us to apply the simplest expression for the uncertainty of the best fit slope [3]:

$$U^2(a_1) = \frac{2 \frac{\sum_{j=1}^{N}\left(m_j - a_1 t_j - a_0\right)^2}{N-2}}{\sum_{j=1}^{N} t_j^2 - \frac{\left(\sum_{j=1}^{N} t_j\right)^2}{N}} = \frac{4\sqrt{3}\, s(m)}{\sqrt{N^3 - N}\, \Delta t} \quad , \tag{10}$$

where a_0 and a_1 are the zeroeth and first-order coefficients of the fit to the mass versus time data. (Here we have used a_1 instead of $\dot{m}$ to avoid confusion: Equation 10 gives the uncertainty related to the fitting process, not the total uncertainty of the mass flow.) The quantity $s(m)$ is the sample standard deviation of the mass fit residuals and Δt is the time interval between successive mass measurements. We used the sample data sets shown in Figure 11 (and others) and found that $s(m)$ ranged from 2 µg at the lowest flows to 12 mg at 100 µL/min. We applied Equation 10 with these values of $s(m)$, $N = 150$, and $\Delta t = 0.39861$ s and found that the uncertainty introduced by the slope calculation is negligible.
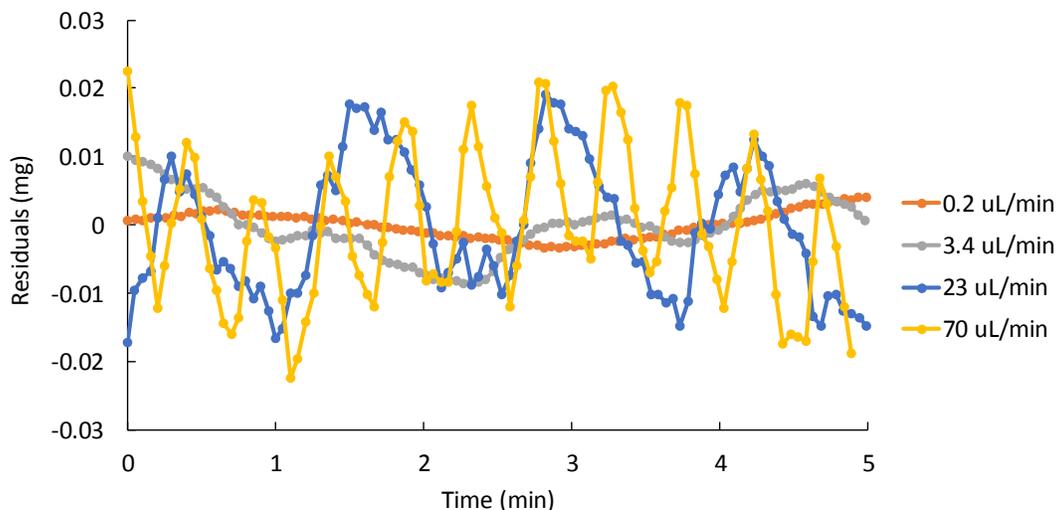
Figure 11. Residuals of first-order best-fits to mass measurements for flows from 0.2 µL/min to 70 µL/min. The periodic flow changes visible for the larger flows are probably caused by the syringe pump.

Evaporation Correction: Water evaporates from the liquid bridge between the pipette and the capillary and through the crevices of the beaker lid (Figures 3 and 4). The relative humidity under the balance wind screen is normally greater than 90 %. However, evaporation of the water in the beaker is significant, about -0.01 µL/min. After completion of all non-zero flow set points, the gravimetric standard continues to acquire data at a no-flow condition, often for many hours, to determine the evaporation correction. An example is shown in Figure 12. The standard uncertainty of the evaporation correction is 0.002 µL/min and this is the most significant uncertainty component at flows < 6 µL/min.
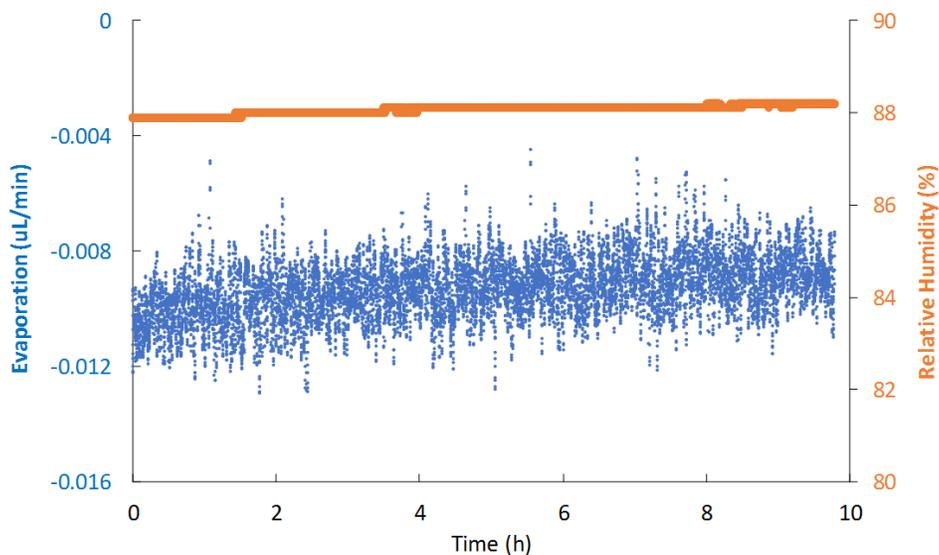

Figure 12. A sample of evaporation and relative humidity data collected at the end of a calibration run.

Flow Stability and Repeatability of the Best Existing Device: Removing air bubbles from the flow tubes is essential for good flow stability. Figure 13a shows large flow transients caused by bubbles alternately moving or sticking in the flow tubes while Figure 13b shows good flow stability when bubbles are removed. The response time of the system to step changes of the flow is markedly faster without air bubbles. Bubbles can be pushed out of the tubing by the operator using the syringe pump when the system is filled, but they

are often not easy to see. The de-bubbler is helpful too. Bubbles can be pulled into the flow tubes though loose fittings during negative flow when the pressure in the system is less than ambient pressure. Data traces like Figure 13a do not produce reliable calibration data and lead to re-testing.
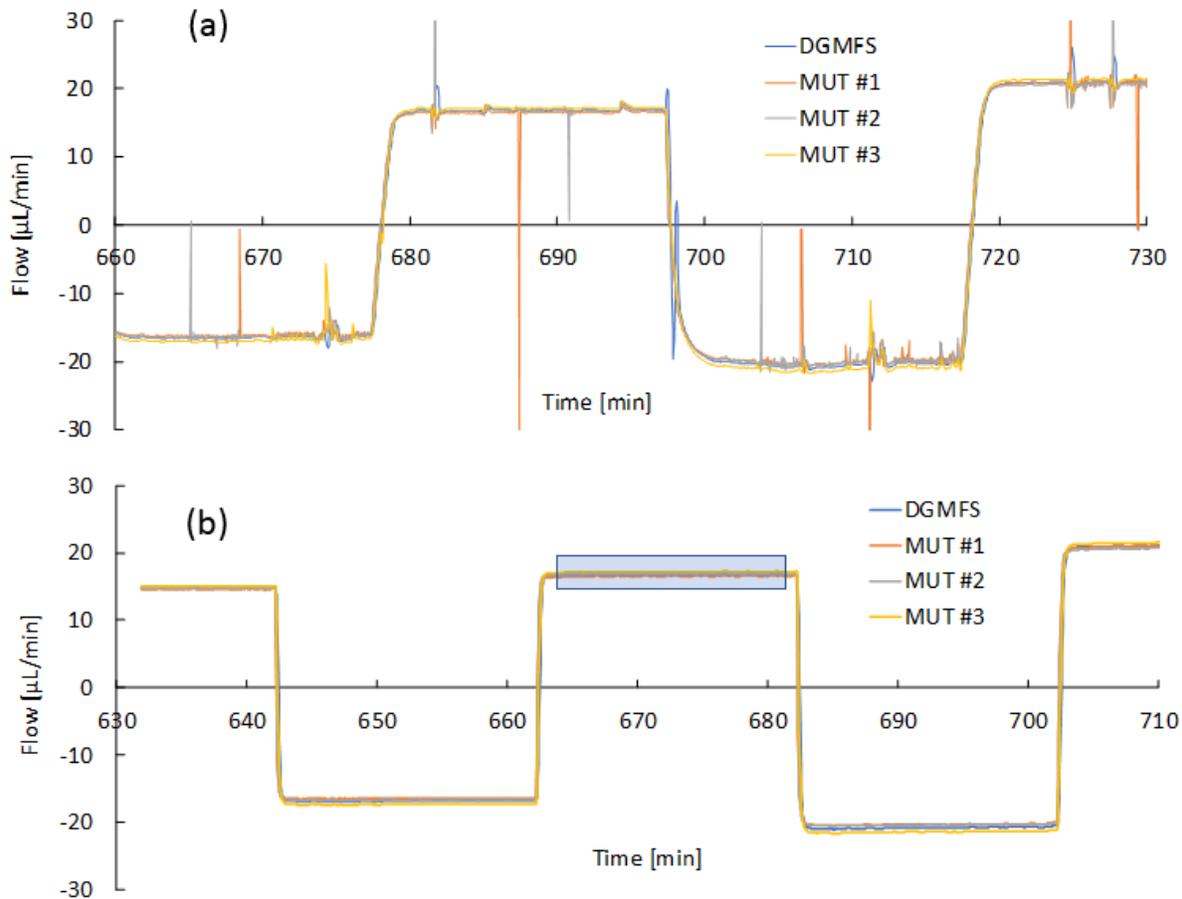

Figure 13. Flow records from the gravimetric standard and three MUTs (a) with air bubbles in the flow tubes and (b) without air bubbles. The data in the rectangular highlight in (b) are plotted on an expanded scale in Figure 14.

Periodic flow changes in the gravimetric standard and three meters under test are clear in Figure 14 (and Figure 11). Bissig [4] notes that, for periodic flows in micro-flow systems, time delays occur between the flows in the pump, the MUT, and the flow standard. When the flow reverses, the pressure distribution in the flexible flow tubes changes and the volumes of the tubes changes. The time required for the flow to adjust to the volume changes is not negligible. In Figure 14, the time delay between the gravimetric standard and the MUTs is approximately 9 s. Other time delays may be caused by the slope calculation using a 20 s moving window, and by the response time of the MUT. These time delays and the finite time response of the flow meters can lead to uncertainty in the flow calibration results. Most flow standards avoid these concerns by providing very steady flow conditions and by using long averages that span many periods of flow fluctuations, but that is more difficult to achieve in micro-flow systems. This subject deserves more attention, especially so that micro-flow applications that need reliable transient flow measurements are well served.

For this uncertainty analysis, we will assume that the uncertainty due to flow instability and time response is captured by the type A repeatability component. Here we use the standard deviation of the 5 repeated

flow measurements from the best existing device. When performing a customer calibration, we use the repeatability for the meter under test instead of the repeatability for the best existing device.
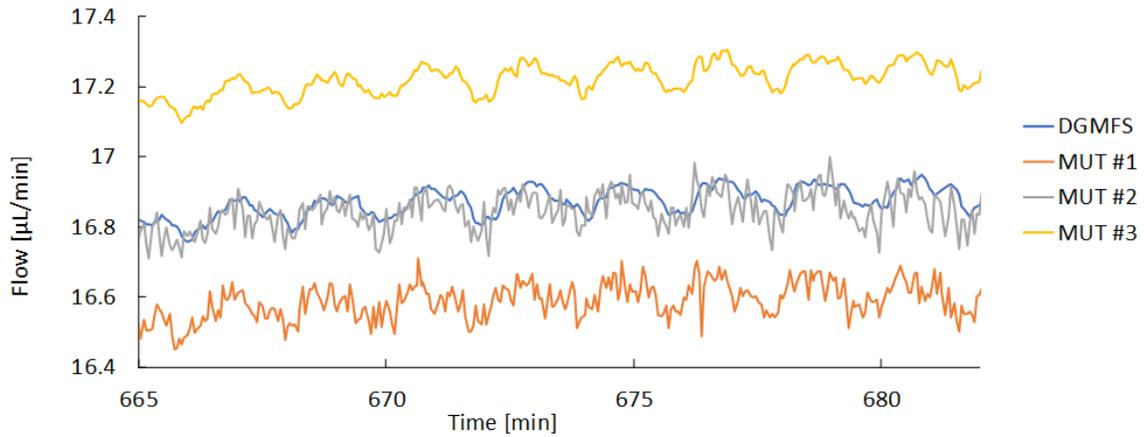

Figure 14. Periodic flow changes, probably caused by mechanical imperfections of the syringe pump drive screw or plunger.

5. Reproducibility of Micro-Flow Meters

The DGMFS was used to calibrate 5 NIST-owned, commercially-purchased flow meters multiple times. We identify these meters by the letters A, B, C, D, and E. Control charts are plotted in the following figures with the flow axis plotted on 1) a linear scale and 2) a log scale. The manufacturer's specification is shown as dashed lines.
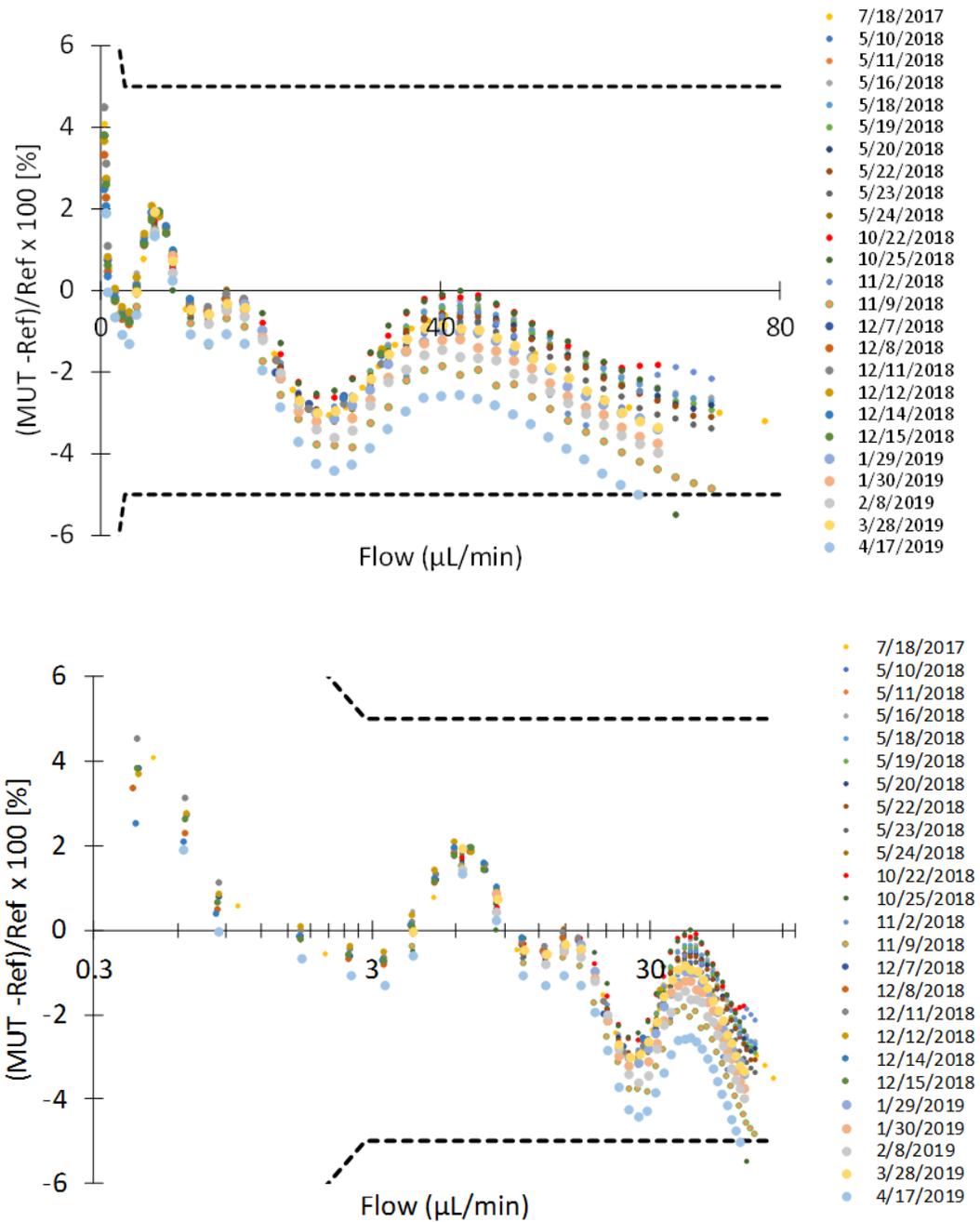
Figure 15. Thermal flow meter A with a 21 month long calibration history, has an error curve than could be well fit with a polynomial or a spline. The scatter of the calibration curves from 25 calibrations over 21 months has standard deviation of about 1.5 %. The calibration data shown here have a turndown ratio of 360 to 1.
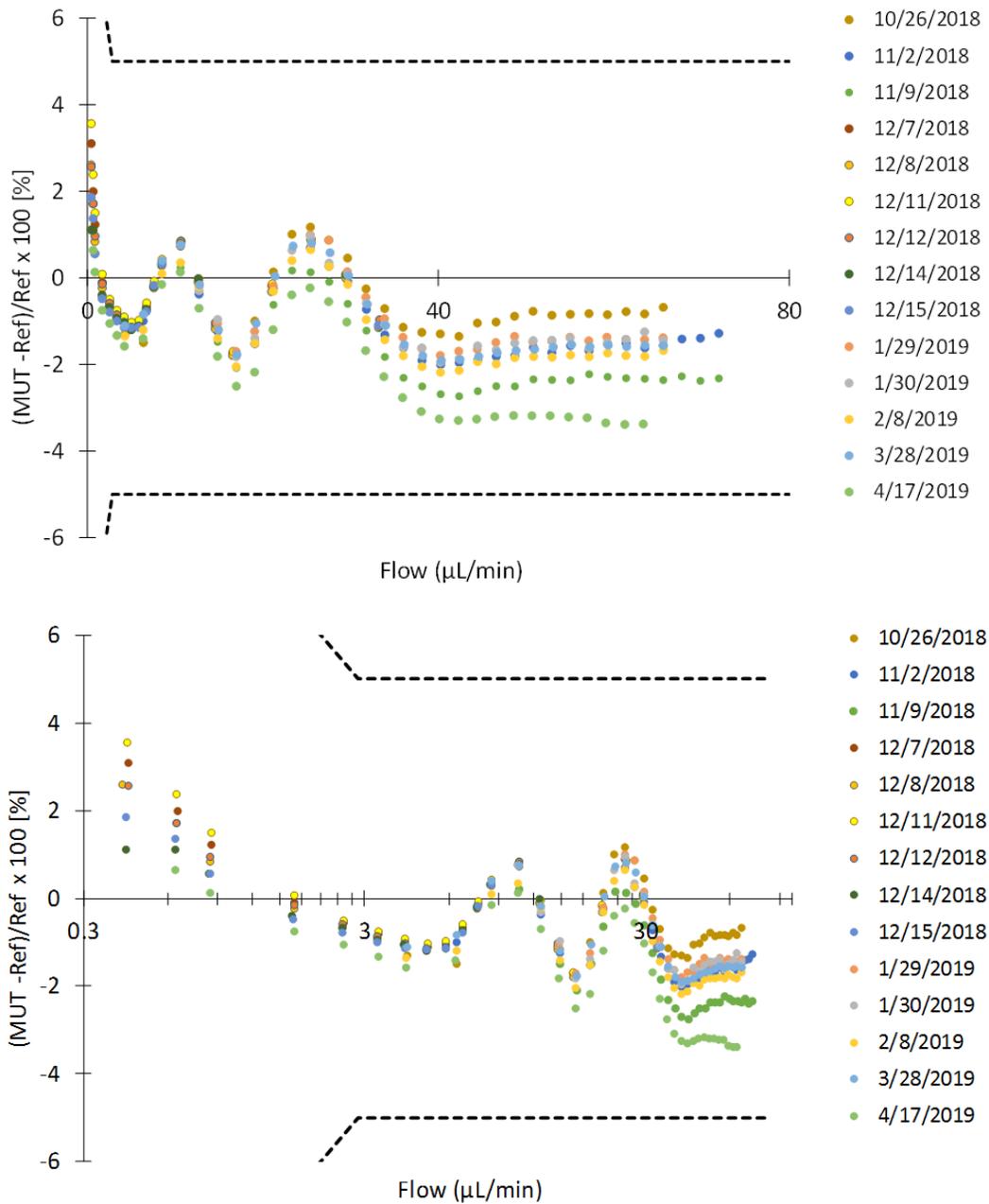
Figure 16. Thermal flow meter B. This meter is the same model as Meter A (Fig. 15.) The meter's 14 calibrations spanning a 6 month period show standard deviations up to 1.4 %.
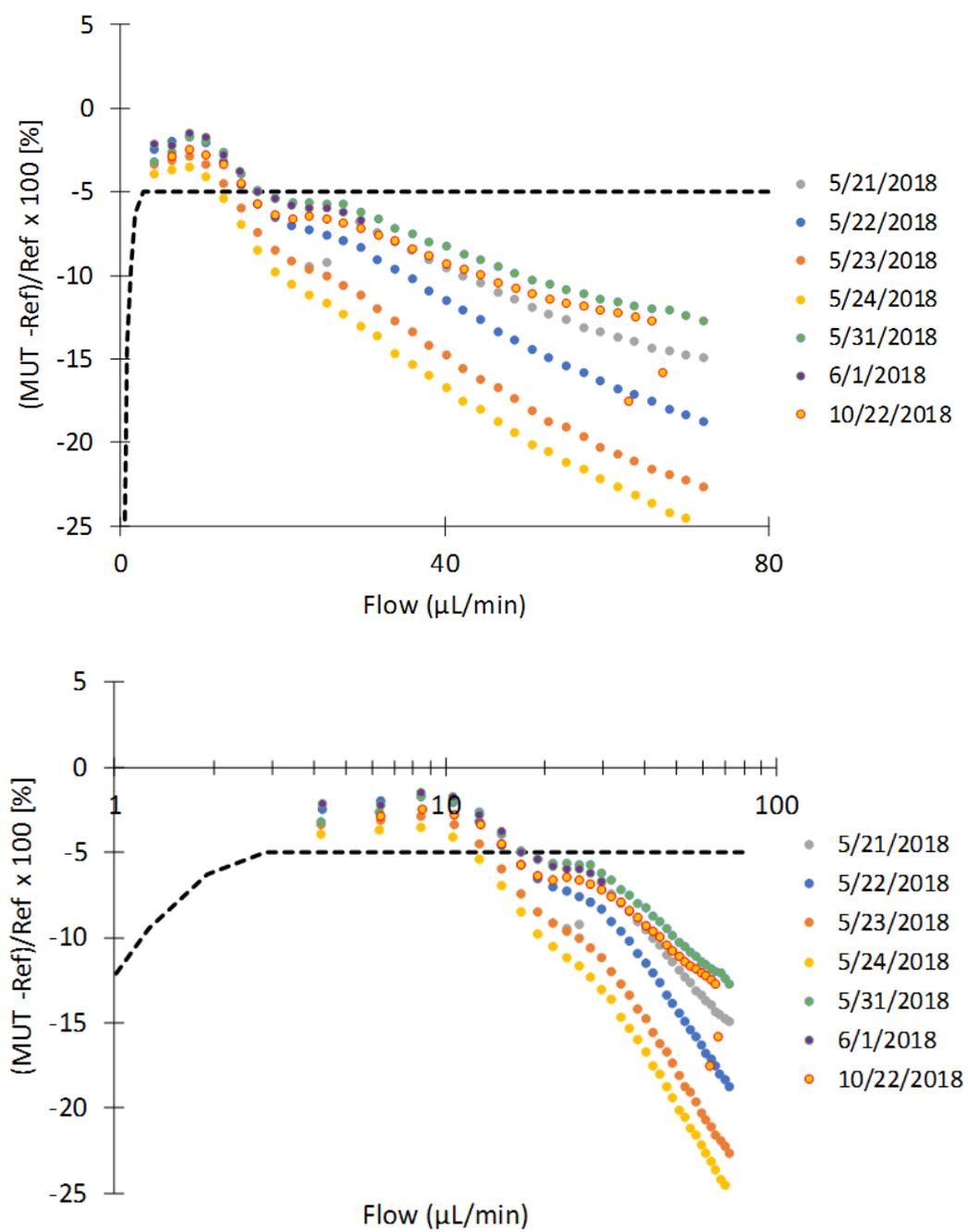
Figure 17. Thermal flow meter C. The calibration of this meter drifted significantly for unknown reasons. This meter was calibrated in series with other MUTs that did not show significant drift. (We always use a check meter in series with the MUT to alert us to possible problems with the DGMFS.)
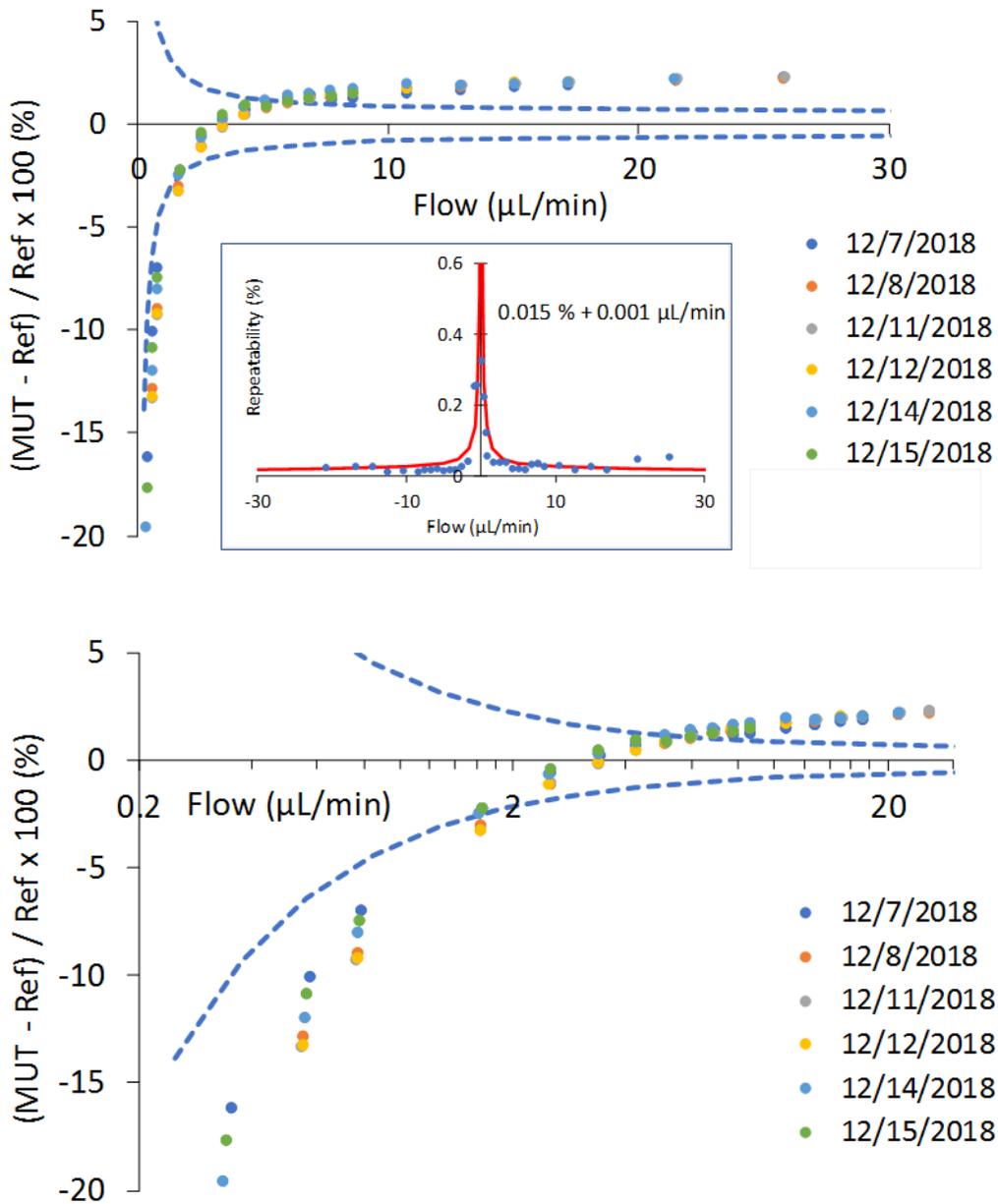
Figure 18. Coriolis flow meter D. These 6 calibrations over a 1-week interval have reproducibility of < 0.5 % over a 16 to 1 turndown ratio. We used meter D to quantify type A uncertainties for the DGMFS uncertainty analysis. The inset is a plot of the repeatability (standard deviation) of the 5 one minute averages for each

set point on 12/8/2018. This meter was not re-zeroed, an easy process that would improve its measurements at low flows.
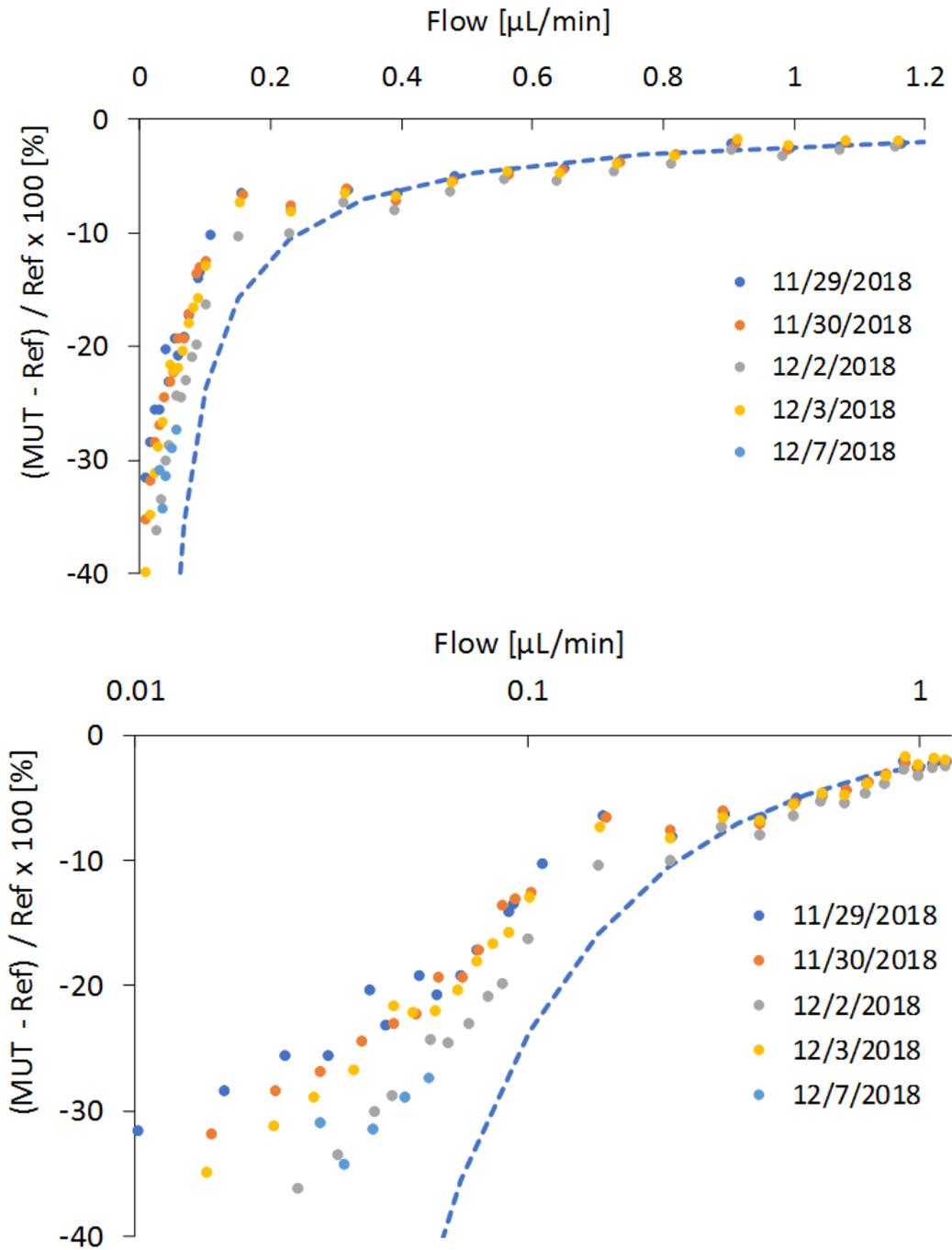

Figure 19. Thermal flow meter E. Meter E was not re-zeroed. If we followed this easy procedure, the results at low flows would improve.

6. Summary and Conclusions

Since it was first commissioned in 2015, NIST's Dynamic Gravimetric Micro-Flow Standard (DGMFS) has been improved by using a liquid bridge between the pipette and the collection beaker, and by the addition of an evaporation trap, camera, and pipette positioning equipment. The liquid bridge avoids varying surface forces on the balance due to stick / slip phenomena on a gradually immersed tube.

A detailed derivation of the equations of flow (based on a force balance) was presented. We showed experimental results quantifying the uncertainty components of mass, time, pipette hydrostatic correction, evaporation, slope calculation, and repeatability. The DGMFS measures water flow between 0.1 μL/min and 100 μL/min with uncertainty ranging from 4.5 % to 0.04 %. At high flows, MUT repeatability and pipette hydrostatic corrections are the largest uncertainties. At low flows, evaporation corrections and repeatability of the best existing device are the largest uncertainty components. We have used the DGMFS at flows as low as 0.01 μL/min (Figure 19), but at that flow, the uncertainty of the standard is estimated to be 45 %, the evaporation correction is equal to the flow, and the k = 2 uncertainty of the evaporation correction is 40 % of the flow. So, until we can reduce the evaporation and its uncertainty, 0.1 μL/min is the practical lower limit of the DGMFS.

Repeated calibrations of five commercially available micro-flow meters (one for nearly 2 years) show that their calibration generally remains stable within 1.5 % for many months. The calibrations show that the flow uncertainty achieved in a user's application can be improved by applying a correction equation based on a calibration against a reference flow standard.

---

[1] Schmidt, J. W. and Wright, J. D., *Micro-Flow Calibration Facility at NIST*, Proceedings of the 9th International Symposium on Fluid Flow Measurement, Arlington, VA, USA, April 14 to 17, 2015.

[2] Jaeger, K. B. and Davis, R. S., *A Primer for Mass Metrology*, NBS Special Publication 700-1, November, 1984.

[3] Coleman, H. W., and Steele, W. G., *Experimentation, Validation, and Uncertainty Analysis for Engineers*, 3rd edition, A. John Wiley and Sons, 2009, Appendix E.

[4] Bissig, H., Tschannen, M., de Huu, M., *Traceable Response Time Characterization in Fast Changing Flow Rates*, Proceedings of the 10th International Symposium on Fluid Flow Measurement, Querétaro, Mexico, March 21 to 23, 2018.